Numerical Heat Transfer, Part A: Applications
An International Journal of Computation and Methodology

ISSN: (Print) (Online) Journal homepage: https://www.tandfonline.com/loi/unht20

Heat transfer in magnetohydrodynamic Jeffery–Hamel molybdenum disulfide/water hybrid nanofluid flow with thermal radiation: A neural networking analysis

T. N. Tanuja, L. Kavitha, Khalil Ur Rehman, Wasfi Shatanawi, S. V. K. Varma & G. V. Kumar

To cite this article: T. N. Tanuja, L. Kavitha, Khalil Ur Rehman, Wasfi Shatanawi, S. V. K. Varma & G. V. Kumar (08 Jan 2024): Heat transfer in magnetohydrodynamic Jeffery–Hamel molybdenum disulfide/water hybrid nanofluid flow with thermal radiation: A neural networking analysis, Numerical Heat Transfer, Part A: Applications, DOI: 10.1080/10407782.2023.2300744

To link to this article: https://doi.org/10.1080/10407782.2023.2300744

Published online: 08 Jan 2024.

NUMERICAL HEAT TRANSFER, PART A: APPLICATIONS
https://doi.org/10.1080/10407782.2023.2300744

Taylor & Francis
Taylor & Francis Group

Heat transfer in magnetohydrodynamic Jeffery–Hamel molybdenum disulfide/water hybrid nanofluid flow with thermal radiation: A neural networking analysis

T. N. Tanuja[a,*], L. Kavitha[a], Khalil Ur Rehman[b], Wasfi Shatanawi[b,c], S. V. K. Varma[a], and G. V. Kumar[d]

[a]Department of Mathematics, School of Applied Sciences, REVA University, Bengaluru, India; [b]Department of Mathematics and Sciences, College of Humanities and Sciences, Prince Sultan University, Riyadh, Saudi Arabia; [c]Department of Mathematics, Faculty of Science, The Hashemite University, Zarqa, Jordan; [d]Department of Mathematics, CSSR & SRRM Degree & PG College, Kamalapuram, India

ABSTRACT

The heat transfer aspects are considered in the Jeffery–Hamel hybrid nanofluid flow between non-parallel plates. In a flow regime, molybdenum disulfide nanoparticles are suspended with a viscous dissipation, magnetic field, and thermal radiation effects. The flow is theoretically modeled, and the differential transformed approach is used to solve the problem. The flow field of the hybrid nanofluid is investigated for different parameters. For the Nusselt number, a sample of 75 values is gathered and compared to five inputs. Fifty-three (70%) values are taken into account for training the neural network. For testing and validating the artificial neural network (ANN) model, 11 (15%) each is used. Using Levenberg–Marquardt backpropagation, the training is carried out. It is noticed that the temperature of MoS_2–MWCNTs/H_2O is higher in comparison with MoS_2/H_2O. Further, according to ANN prediction, Pr, Ec, and *M* have a growing relationship with the Nusselt number; however, Re and Nr have an opposite relationship.

ARTICLE HISTORY
Received 17 April 2023
Revised 21 December 2023
Accepted 26 December 2023

KEYWORDS
Heat transfer; Jeffery–Hamel flow; thermal radiation; differential transform method; hybrid nanofluid; neural networking

1. Introduction

The heat transfer aspects in fluid flow between diverging and convergent channels own a wide range of applications in many engineering fields. To be more specific about the flow between divergent and convergent channels, according to Jeffery [1] and Hamel [2], a Jeffery–Hamel flow is a two-dimensional flow between converging or diverging channels that are positioned apart from one another by an inclination and is driven by a line sink or source at the apex. It claims numerous applications, mainly in aerospace engineering, chemical reactors [3], plasma originators [4], intensifying or constricting machines regions [5], compressors of gas [6], and pipe sections [7]. Many researchers solved the problem of Jeffery–Hamel flow by using different approaches such as the perturbation technique [8], the homotopy perturbation technique [9–11], and the Adomain decomposition method [12], and our work is analogous with these methods.

Various investigations exist for the problem of a viscous fluid with magnetohydrodynamic (MHD) flow under different conditions [13–15]. Umavathi and Shekar [16] discussed the Jeffery–Hamel flow delinquent by employing the differential transform method (DTM) and considered

CONTACT Khalil Ur Rehman kurrehman@psu.edu.sa Department of Mathematics and Sciences, College of Humanities and Sciences, Prince Sultan University, Riyadh 11586, Saudi Arabia.
*Department of Mathematics, CHRIST University, Bengaluru, India.

Nomenclature

C_p	dynamic viscosity
Ec	Eckert number
k	thermal conductivity
$\bar{k}$	mean absorption coefficient
M	magnetic field
Nr	radiation parameter
P	pressure
Pr	Prandtl number
Re	Reynolds number
u	velocity of hybrid nanofluid in radial direction

Greek symbols

α	angle of inclination
$\alpha < 0$	convergent channel
$\alpha > 0$	divergent channel
η	dimensionless angle
ρ	density of fluid
$\bar{\sigma}$	Stefan Boltzmann constant
ϕ_1, ϕ_2	solid volume fractions of nanoparticle

Subscripts

f	base fluid
hnf	hybrid nanofluid
s_1, s_2	solid nanoparticles

the magnetic field. Sheikholeslami and coauthors [17] analytically discussed the Jeffery and Hamel nanofluid flow in plates. Ochieng et al. [18] studied the Jeffery–Hamel fluid flow in a diverging channel in the occurrence of a conducting field. By considering Joule's dissipation, Rashid et al. [19] theoretically studied the effect of nanoparticle shapes in between convergent and divergent channels. Khan et al. [20] employed the Range Kutta method to explore the rate of heat transfer of Jeffery–Hamel hybrid nanofluid flow among convergent and divergent channels. Using the DTM technique, Meher and Patel [21, 22] looked into the heat transmission of Cu/water nanofluid in a channel.

By using the Levenberg–Marquardt scheme (LMS) in a backpropagation learning task of an artificial neural network (ANN), Bilal et al. [23] solved the problem of MHD fractional flow of the boundary layer over a permeable stretching sheet. Khan et al. [24] studied the Falkner–Skan heat transfer by using an artificial neural network with the Levenberg–Marquardt method (NN-BLMM) technique. They noticed that velocity increases and thermal boundary layer decreases by increasing the Deborah number. Khan et al. [25] studied the heat and mass transfer characteristics of unstable squeezing flow between parallel plates by developing the feed-forward neural network strength using the Levenberg–Marquardt method (NN-BLMM). A boundary layer flow over a stretching sheet is studied by Ullah and coauthors [26], they developed the code for Feed-forward neural network strength using the Levenberg–Marquardt method (NN-BLMM). They validate the result by comparing Levenberg–Marquardt method (NN-BLMM) with numerical technique. Ullah et al. [27] studied an effective Levenberg–Marquardt algorithm-based ANN model is proposed to discover an exact series solution for micropolar flow in an open channel with mass injection. They obtained the experimental results by using mean square error (MSE) and absolute error metric functions. Ullah et al. [28] studied the effects of both magnetic and electric fields on the velocity of micropolar nanofluid between two parallel plates with rotation under the influence of Hall current have been investigated using ANNs with the Levenberg–Marquardt backpropagation technique. Ullah et al. [29] used the technique neural networks for intelligent computing of the Levenberg–Marquard method for the numerical treatment of squeezing nanofluid flow between two cylindrical plates. By using optimal homotopy analysis with the ANN–LMS method, a validation study is carried out. Ullah et al. [30] studied the flow effects of heat transfer on Maxwell nanofluid flow over a horizontal rotating surface with MHDs using stochastic numerical techniques through ANNs. Also, they considered the effects of thermal energy, concentration, and Brownian motion. Ullah et al. [31] worked on complex fractional PDEs; to solve these Partial Differential Equation (PDE) equations, they developed a semi-analytical method called the optimal auxiliary function method. The advantage of this method is fast convergence.

The nonlinear form of the differential equation has a notable impact in applied mathematics, physics, and engineering fields. Many physical phenomena are modeled using nonlinear differential equations. For these issues, numerical and analytical approaches have been developed to produce precise answers. The computation of solutions for such problems is tedious since these problems have higher-ordered derivatives. Hence, an updated version of Taylor's series method was introduced and it is called the "differential transform method" (abbreviated as DTM). Zhou [32] introduced the DTM in 1986. By using DTM [33, 34], both nonlinear and linear initial value problems in electrical circuit analysis can be solved. Polynomial form solution can be obtained by using this method. DTM is the method of determining the coefficient of Taylor's series of functions by solving an induced recursive equation from the given differential equation. If $p(y)$ is an infinitely and continuously differentiable function, then $p(y)$ can be written in the Taylor series as

$$p(y) = \sum_{x=0}^{\infty} \frac{1}{x!} \frac{\mathrm{d}^x p(y_0)}{dy^x} (y - y_0)^x \tag{1}$$

Define the differential transform of $p(y)$ order x, represented by $P(x)$

$$P(x) = \frac{1}{x!} \frac{\mathrm{d}^x p(y_0)}{dy^x} \tag{2}$$

The inverse differential transforms $P(x)$ can be written as:

$$p(y) = \sum_{x=0}^{\infty} P(x)(y - y_0)^x \tag{3}$$

while the detail of basic operations ad transformed functions is given in Table 1.

We investigate the Jeffery–Hamel flow between non-parallel plates in this study. Heat transfer is taken into account along with viscous dissipation, a magnetic field, and thermal radiation. In a flow regime, molybdenum disulfide nanoparticles are suspended. The flow field between non-parallel plates is modeled theoretically. The DTM approach is used to approximate the solution of a differential equation. The effects of flow parameters are investigated. The Nusselt number is predicted by using an ANN model for five distinct flow characteristics. The format of the article is as follows: Section 1 owns motivation literature survey while Section 2 offers mathematical formulation for flow between the plates and also the solution directory. Results and discussion are debated in Section 3 while ANN formation is given in Section 4. Outcomes are itemized in Section 5.

Table 1. Differential transformed functions and basic operations of DTM.

Basic function	Transfigured function
$z(y) = u(y) \pm v(y)$	$Z(n) = U(n) \pm V(n)$
$z(y) = \alpha u(y)$	$Z(n) = \alpha U(n)$
$z(y) = \frac{du(y)}{dy}$	$Z(n) = (n+1)U(n+1)$
$z(y) = \frac{d^2u(y)}{dy^2}$	$Z(n) = (n+1)(n+2)U(n+2)$
$z(y) = \frac{d^m u(y)}{dy^m}$	$Z(n) = (n+1)(n+2)\cdots\cdots\cdot(n+m)U(n+m)$
$z(y) = u(y)v(y)$	$Z(n) = \sum_{m=0}^{n} U(m)V(n-m)$
$z(y) = \alpha y^m$	$Z(n) = \alpha\delta(n-m)$; where $\delta(n-m) = \begin{cases} 1, & \text{if } m = m \\ 0, & \text{if } n \neq m \end{cases}$

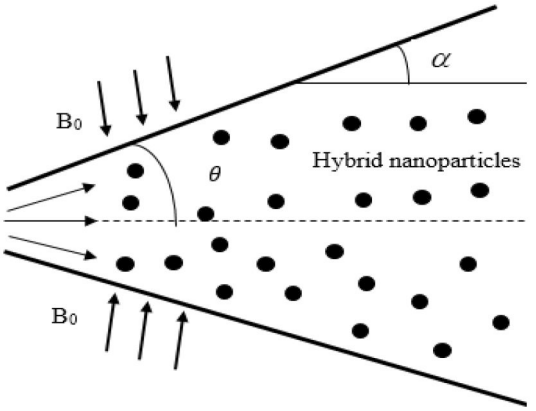

Figure 1. Geometry of flow.

Table 2. Thermophysical properties.

Property	Water	MoS_2	MWCNTs(Multi Wall Carbon Nanotubes)
ρ (kg/m^2)	977.1	5,060	1,600
k (W/mK)	0.613	904.4	3,000
C_p (J/kg K)	4,179	397.21	796

2. Mathematical model

The laminar flow of an incompressible conducting viscous hybrid nanofluid between non-parallel plates is considered. The angle between the wall is assumed to be as shown in Figure 1. The flow is considered to be radial and symmetrical. In this analysis, hybrid nanofluid containing and as nanoparticles and as base fluid is well-thought-out with viscous dissipation and thermal radiation effects. The equations of continuity, momentum, and energy [35] are considered with a magnetic field.

The ultimate flow equations are:

$$\frac{\rho_{hnf}}{r}\frac{\partial(ru)}{\partial r} = 0 \tag{4}$$

$$\frac{\mu_{hnf}}{\rho_{hnf}}\left(\frac{\partial u}{\partial r}\frac{1}{r} + \frac{\partial^2 u}{\partial r^2} + + \frac{\partial^2 u}{\partial \theta^2}\frac{1}{r^2} - \frac{u}{r^2}\right) - u\frac{\partial u}{\partial r} - \frac{1}{\rho_{hnf}}\frac{\partial P}{\partial r} - \frac{\sigma B_0^2}{\rho_{hnf} r^2}u = 0 \tag{5}$$

$$\frac{1}{\rho_{hnf}}\frac{\partial P}{\partial \theta}\frac{1}{r} - \frac{\partial u}{\partial \theta}\frac{2\mu_{hnf}}{\rho_{hnf} r^2} = 0 \tag{6}$$

$$u\frac{\partial T}{\partial r} = \alpha_{hnf}\left(\frac{\partial T}{\partial r}\frac{1}{r} + \frac{\partial^2 T}{\partial r^2} + \frac{\partial^2 T}{\partial \theta^2}\frac{1}{r^2}\right) + \left[\left(\frac{\partial u}{\partial r}\right)^2 + \frac{u^2}{r^2}\right]\frac{2\mu_{hnf}}{(\rho C_p)_{hnf}} + \frac{16\sigma^* T_\infty^3}{3k^*(\rho C_p)_{hnf}}\left(\frac{\partial T}{\partial r}\frac{1}{r} + \frac{\partial^2 T}{\partial r^2} + \frac{\partial^2 T}{\partial \theta^2}\frac{1}{r^2}\right) \tag{7}$$

Boundary conditions for the flow model are given below:

At the axis of the channel: $\frac{\partial u(r,\theta)}{\partial r} = 0,\ \frac{\partial T}{\partial \theta} = 0,\ u(r,\theta) = U$

At the walls of the channel, at the plates: $u(r,\theta) = 0,\ T = T_w$

The Abu-Nada [36] expressions of the hybrid nanofluid parameter such as viscosity, thermal diffusivity, and heat capacitance are considered as follows:

$$\mu_{hnf} = \frac{\mu_f}{(1-\phi_1)^{2.5}(1-\phi_2)^{2.5}}, \alpha_{hnf} = \frac{k_{hnf}}{(\rho C_p)_{hnf}} and (\rho C_p)_{hnf} = (1-\phi_2)\left[(1-\phi_1)\rho_f + \phi_1\rho_1\right] + \phi_2\rho_2 \tag{8}$$

According to Maxwell, hybrid nanofluid thermal conductivity is considered as:

$$k_{hnf} = k_{bf}\left[\frac{k_2 + 2k_{bf} - 2\phi_2(k_{bf} - k_2)}{k_2 + 2k_{bf} + \phi_2(k_{bf} - k_2)}\right], k_{bf} = k_f\left[\frac{k_1 + 2k_f - 2\phi_1(k_f - k_1)}{k_1 + 2k_f + \phi_1(k_f - k_1)}\right] \tag{9}$$

Thermophysical properties for the present problem are given in Table 2. Since only radial flow is considered, Eq. (4) becomes:

$$f(\theta) = ru(r,\theta) \tag{10}$$

Dimensionless parameters

$$f(\eta) = \frac{f(\theta)}{f_{\max}}, \quad f_{\max} = rU, \quad \eta = \frac{\theta}{\alpha}, \quad \xi(\eta) = \frac{T}{T_w}, \quad \mathrm{Nr} = \frac{16T_\infty^3\sigma^*}{k_f k^*} \tag{11}$$

By eliminating pressure in between Eqs. (5) and (6), we get:

$$f'''(\eta) + 2\alpha \mathrm{Re} A_1 B_1 f(\eta) f'(\eta) + \left(4 - B_1 M^2\right)\alpha^2 f'(\eta) = 0 \tag{12}$$

$$\frac{1}{A_2}\left[\xi''(\eta)(A_3 + Nr) + \frac{\mathrm{PrEc}}{B_1}\left(4\alpha^2 f(\eta)^2 + f'(\eta)^2\right)\right] = 0 \tag{13}$$

Dimensionless boundary conditions are:

$$\begin{gathered} f'(0) = 0, \quad f(0) = 1, \quad f(1) = 0, \\ \xi'(0) = 0, \quad \xi(1) = 1. \end{gathered} \tag{14}$$

2.1. Solution by DTM

Eq. (12) becomes

$$\begin{aligned} &((m+3)(m+2)(m+1))F(m+3) + 2\alpha \mathrm{Re} A_1 B_1 \sum_{i=0}^{m}(m-i+1)F(i)F(m-i+1) \\ &\quad + \left(4 - B_1 M^2\right)\alpha^2 (m+1)F(m+1) = 0 \end{aligned} \tag{15}$$

Eq. (13) becomes

$$\frac{1}{A_2}\left[(m+2)(m+1)\Theta(m+2)(A_3 + \mathrm{Nr}) + \frac{\mathrm{PrEc}}{B_1}\left(\begin{array}{c} 4\alpha^2 \sum_{i=0}^{m} F(i)F(m-i) \\ + \sum_{i=0}^{m}(i+1)(m-i+1)F(i+1)F(m-i+1) \end{array}\right)\right] = 0 \tag{16}$$

Converted boundary parameters are:

$$F(0) = 1, \quad \Theta(1) = 0, \quad F(1) = 0, \tag{17}$$

$$\sum_{i=0}^{\infty}\Theta(i) = 1, \quad \sum_{i=0}^{\infty}F(i) = 0, \tag{18}$$

Considering initial values $F(2)=\delta,\ \Theta(0)=\beta$, Eqs. (15) and (16) with modified boundary conditions are used to solve a system of algebraic equations and determine the unknowns α and β. The obtained solutions are given below:

- For velocity:

$$F[3]=0$$

$$F[4]=\frac{1}{12}\left(-4\alpha^2\delta+M^2\alpha^2\delta B_1-2\mathrm{Re}\alpha\delta A_1B_1\right)$$

$$F[5]=0$$

$$F[6]=\frac{1}{30}\left(-4\alpha^2F[4]+M^2\alpha^2F[4]B_1-\mathrm{Re}\alpha\delta^2A_1B_1-2\mathrm{Re}\alpha F[4]A_1B_1\right)\ \textit{and so on.} \tag{19}$$

- For temperature:

$$\Theta[2]=\frac{-2Ec\mathrm{Pr}\alpha^2}{B_1(A_3+Nr)}$$

$$\Theta[3]=0$$

$$\Theta[4]=\frac{-Ec\mathrm{Pr}(2\alpha^2\delta+\delta^2)}{3B_1(A_3+Nr)}$$

$$\Theta[5]=0$$

$$\Theta[6]=\frac{-2\mathrm{EcPr}\left(\alpha^2\delta^2+2\alpha^2F[4]+4\delta F[4]\right)}{15B_1(A_3+\mathrm{Nr})} \tag{20}$$

As the process is continuous, the following equations may be obtained by replacing the primary Eq. (18) based on the DTM process with Eqs. (19) and (20):

$$f(\eta)=1+\delta\eta^2+\frac{1}{12}\begin{pmatrix}-4\alpha^2\delta+M^2\alpha^2\delta B_1\\-2\mathrm{Re}\alpha\delta A_1B_1\end{pmatrix}\eta^4+\frac{1}{30}\begin{pmatrix}-4\alpha^2F[4]+M^2\alpha^2F[4]B_1\\-\mathrm{Re}\alpha\delta^2A_1B_1-2\mathrm{Re}\alpha F[4]A_1B_1\end{pmatrix}\eta^6+\cdots\cdots \tag{21}$$

$$\xi(\eta)=\beta-\frac{2\mathrm{EcPr}\alpha^2}{B_1(A_3+\mathrm{Nr})}\eta^2-\frac{\mathrm{EcPr}(2\alpha^2\delta+\delta^2)}{3B_1(A_3+\mathrm{Nr})}\eta^4-\frac{2\mathrm{EcPr}\left(\alpha^2\delta^2+2\alpha^2F[4]+4\delta F[4]\right)}{15B_1(A_3+\mathrm{Nr})}\eta^6+\cdots \tag{22}$$

To obtain initial values δ and β we substitute Eqs. (21) and (22) in Eq. (18) with $\eta=1$, then

$$f(1)=1+\delta+\frac{1}{12}\begin{pmatrix}-4\alpha^2\delta+M^2\alpha^2\delta B_1\\-2\mathrm{Re}\alpha\delta A_1B_1\end{pmatrix}+\frac{1}{30}\begin{pmatrix}-4\alpha^2F[4]+M^2\alpha^2F[4]B_1\\-\mathrm{Re}\alpha\delta^2A_1B_1-2\mathrm{Re}\alpha F[4]A_1B_1\end{pmatrix}+\cdots\cdots=0 \tag{23}$$

$$\xi(1)=\beta-\frac{2\mathrm{EcPr}\alpha^2}{B_1(A_3+\mathrm{Nr})}-\frac{\mathrm{EcPr}(2\alpha^2\delta+\delta^2)}{3B_1(A_3+\mathrm{Nr})}-\frac{2\mathrm{EcPr}\left(\alpha^2\delta^2+2\alpha^2F[4]+4\delta F[4]\right)}{15B_1(A_3+\mathrm{Nr})}+\cdots\cdots=1 \tag{24}$$

- Derived quantities
  Expression of skin friction coefficient (τ) and shear stress (τ_w) are:

$$\tau = \frac{\tau_w}{\rho_f U_{\max}^2} \tag{25}$$

$$\tau_w = \mu_{hnf}\left(\frac{1}{r}\frac{\partial u}{\partial \theta}\right) \tag{26}$$

Substituting Eq. (11) into Eqs. (25) and (26) yields:

$$\tau = \frac{1}{\mathrm{Re}(1-\phi_1)^{2.5}(1-\phi_2)^{2.5}} f'(1) \tag{27}$$

Expression of heat flux and Nusselt number gives:

$$q_w = \left(k_{hnf} + \mathrm{Nr}\right)\frac{1}{r}\frac{\partial T}{\partial \theta} \tag{28}$$

$$\mathrm{Nu} = \frac{r q_w|_{\theta=\alpha}}{k_f T_w} \tag{29}$$

By using Eq. (11) in Eqs. (28) and (29), we get:

$$\mathrm{Nu} = -\frac{1}{\alpha}\frac{k_{hnf}}{k_f}\xi'(1) \tag{30}$$

3. Results and discussion

3.1. Analysis of results

The mathematical theories of the DTM and ANN provide highly accurate solutions for the boundary value problem, which are presented in Section 2. The solution is obtained by using DTM method. We have used MATLAB for our computational work. The results obtained are compared with predicted values for Nusselt numbers and actual values using ANNs. From Figures 2–11, the effects of fluid flow parameters and derived quantities such as Nusselt number and skin friction are studied by using DTM and from Figures 12–15, the effects of various parameters of fluid flow and the effect of Nusselt number are studied by using the ANN model.

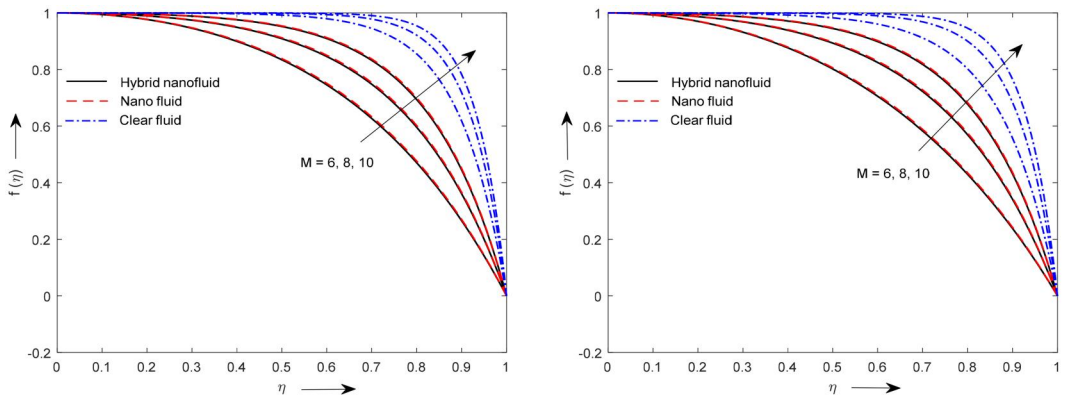

Figure 2. Velocity profiles of the convergent and divergent channel with magnetic field.

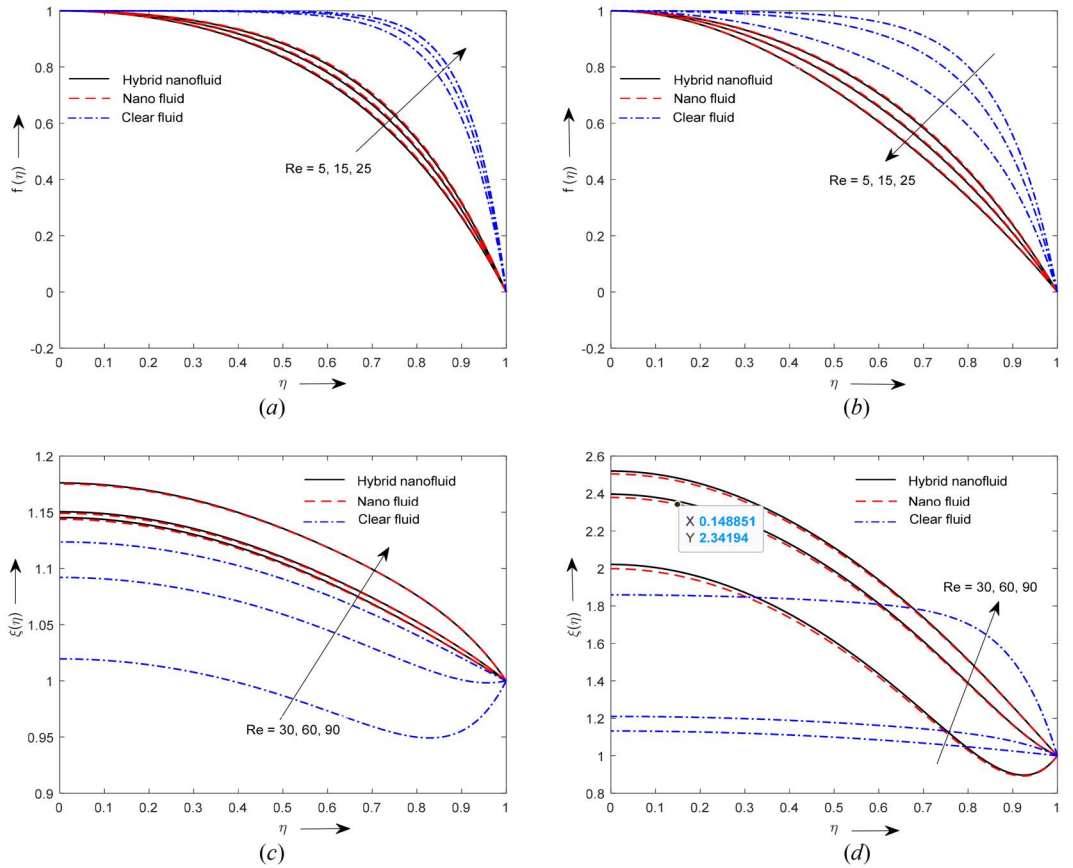

Figure 3. Velocity profiles of convergent (*a*) and divergent (*b*) channels and temperature profile of convergent (*c*) and divergent (*d*) channels for various Reynolds numbers.

Table 3 denotes the water Prandtl number for atmospheric pressure at different temperatures. Table 4 gives the performance parameter for the ANN model.

3.2. Discussion of results

The heat transfer in Jeffery–Hamel flow of hybrid nanofluid with a conducting field and thermal radiation are studied in both divergent and convergent channels. There are numerous techniques [37–39] for resolving flow equations but in the present problem, the equations are nonlinear and resolved by using DTM. In detail, Figure 2 shows the velocity in both divergent and convergent channels for various values of magnetic field (M) for a hybrid nanofluid, a nanofluid, and a base fluid. The flow rate of the base fluid is higher than the nanofluid (MoS_2/H_2O). Hybrid nanofluid (MoS_2–MWCNTs/H_2O) velocity is less than the nanofluid. It is observed that as a magnetic field (M) increases, the velocity increases, it is since the magnetic field enhances viscous forces, which results in increasing the resistance.

The impact of the Reynolds number on the flow rate and temperature of the fluid can be observed in Figure 3. Graphs are plotted for increasing values of the Reynolds number for both $\alpha > 0$ and $\alpha < 0$ channels. Velocity declines for higher Reynolds number, this trend is observed in the divergent channel. Velocity increases with an increment in Re in the convergent canal. The ratio of the inertial and viscous forces, where the fluid velocity and the boundary layer are improved, is physically represented by the Re. The heat transfer rate rises with an increase in Re

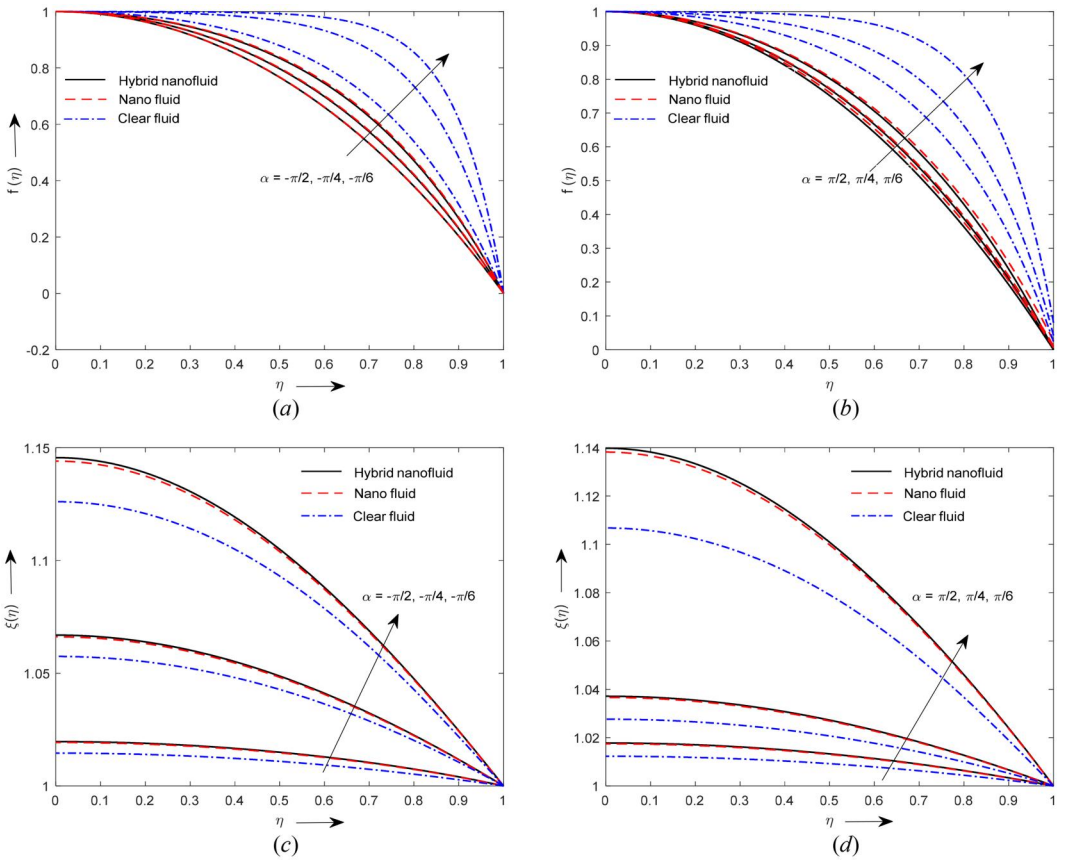

Figure 4. Velocity profiles of convergent (*a*) and divergent (*b*) channels and temperature profile of convergent (*c*) and divergent (*d*) channels for various values of α.

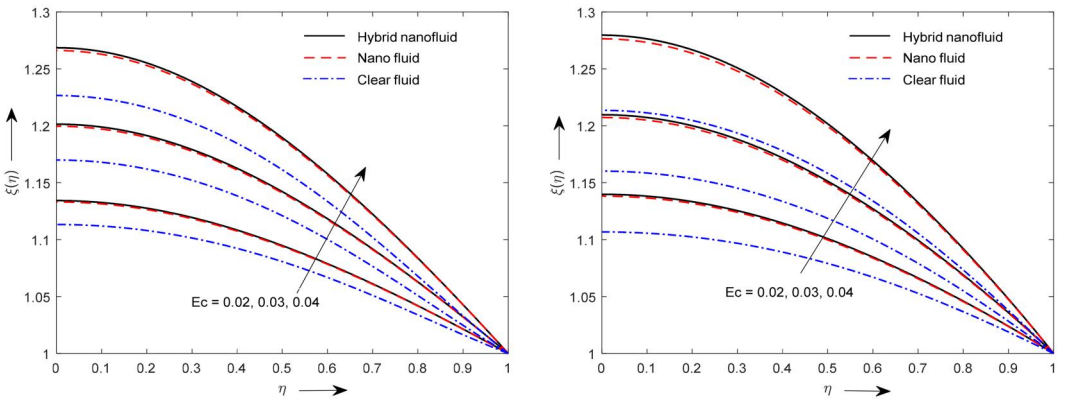

Figure 5. Temperature profiles of the convergent and divergent channel with Eckert number.

in both channels. Due to its greater thermal conductivity than nano- and base-fluid counterparts, hybrid nanofluid has a higher temperature than the nanofluid.

Figure 4 illustrates the impacts of the angle of inclination on the flow rate and temperature profiles for both channels. As a result, the larger the value α results in greater the temperature and velocity. Physically, the effect of the wall on the flow rate decrease as the angle of inclination upsurges. The flow of the base fluid is higher when compared to hybrid and nanofluid. Hybrid

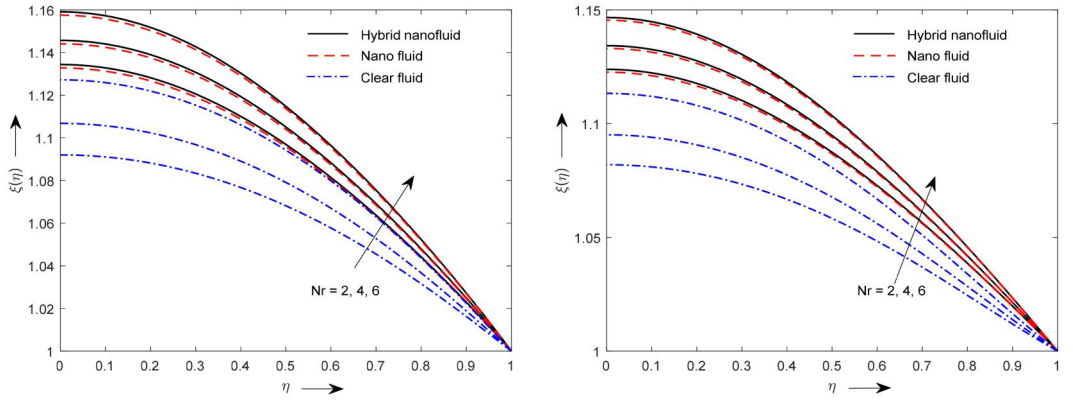

Figure 6. Temperature profiles of the convergent and divergent channel with thermal radiation.

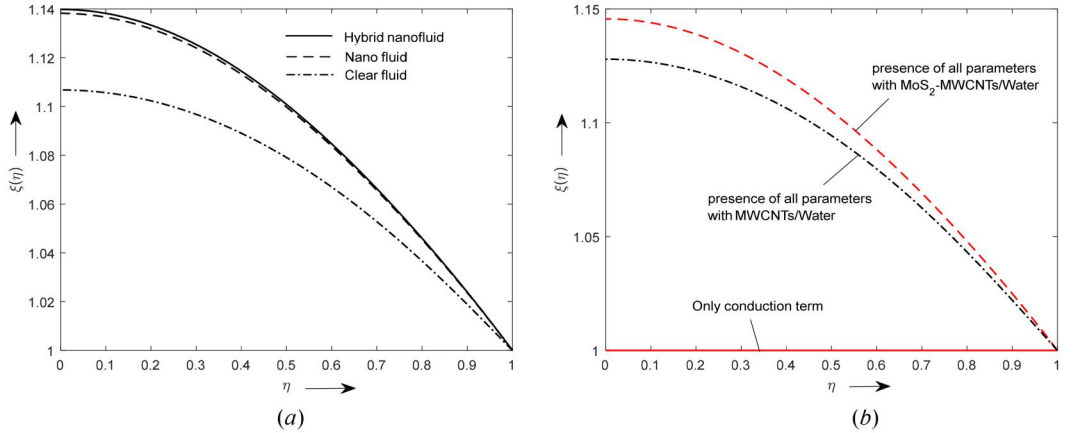

Figure 7. Comparison graph for hybrid, nano- and clear fluid.

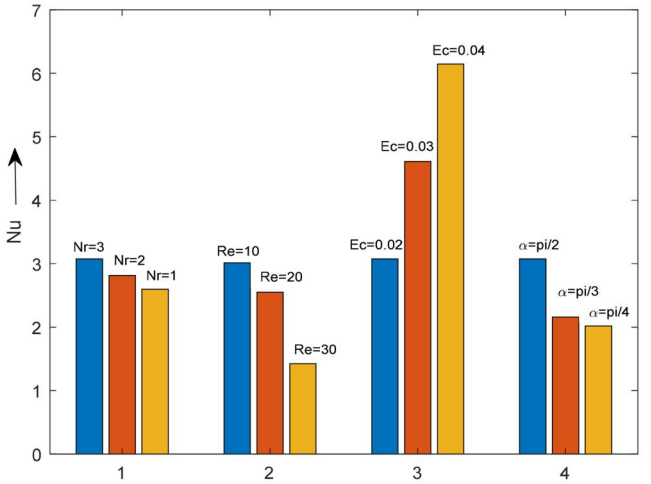

Figure 8. Nusselt number graph for variation in Nr, Re, Ec, and α.

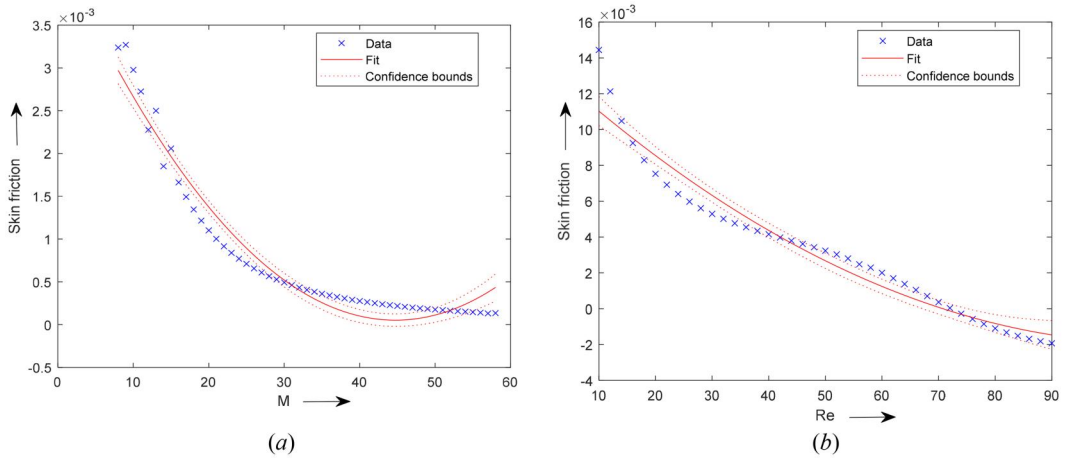

Figure 9. Quadratic regression graph for magnetic field and Reynolds number.

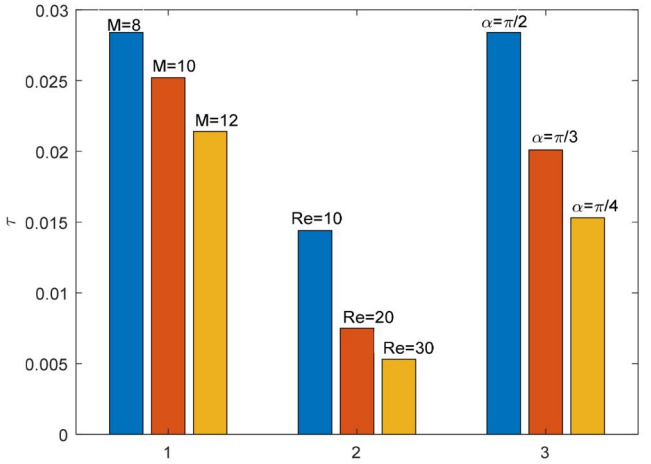

Figure 10. Skin friction graph for variation in M, Re, and α.

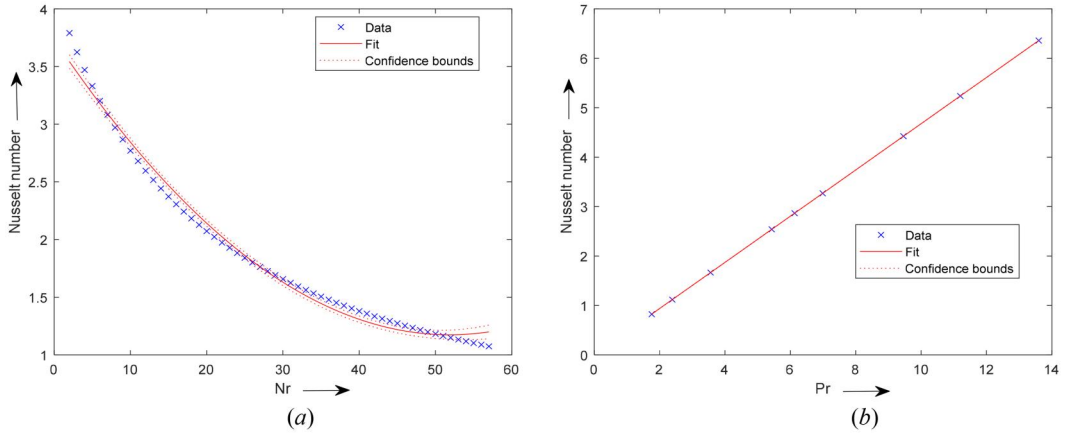

Figure 11. Quadratic regression graph for thermal radiation and various values of Prandtl number.

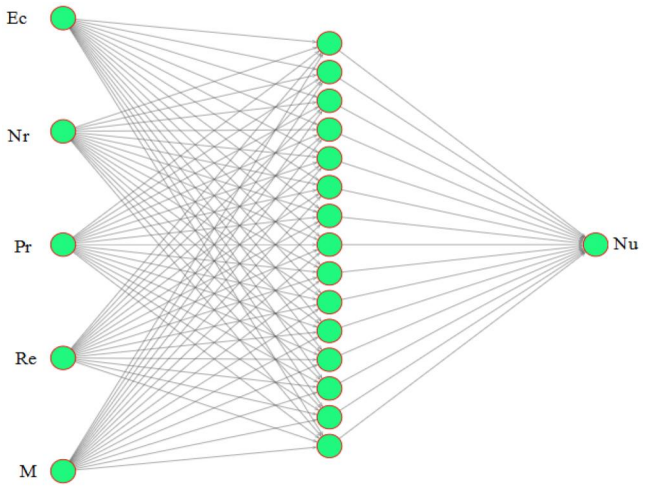

Figure 12. Architecture of neural network.

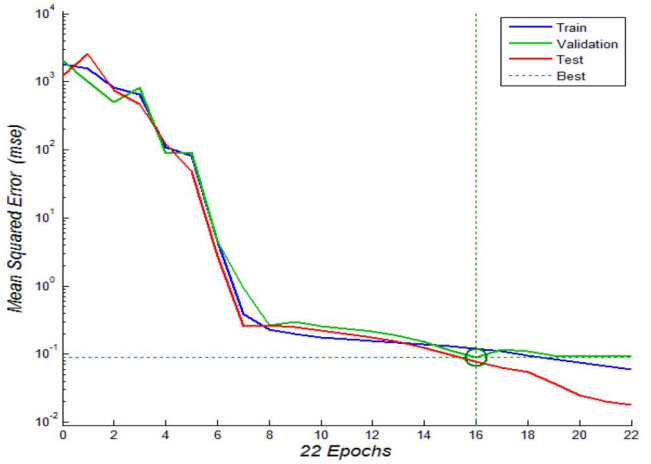

Figure 13. Performance of neural network.

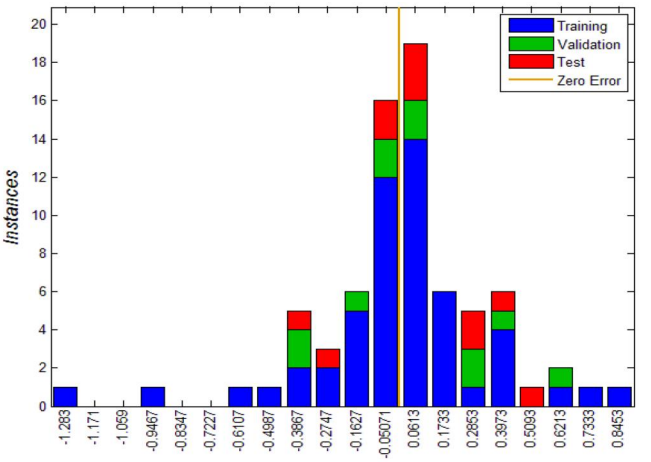

Figure 14. Error histogram of neural network.

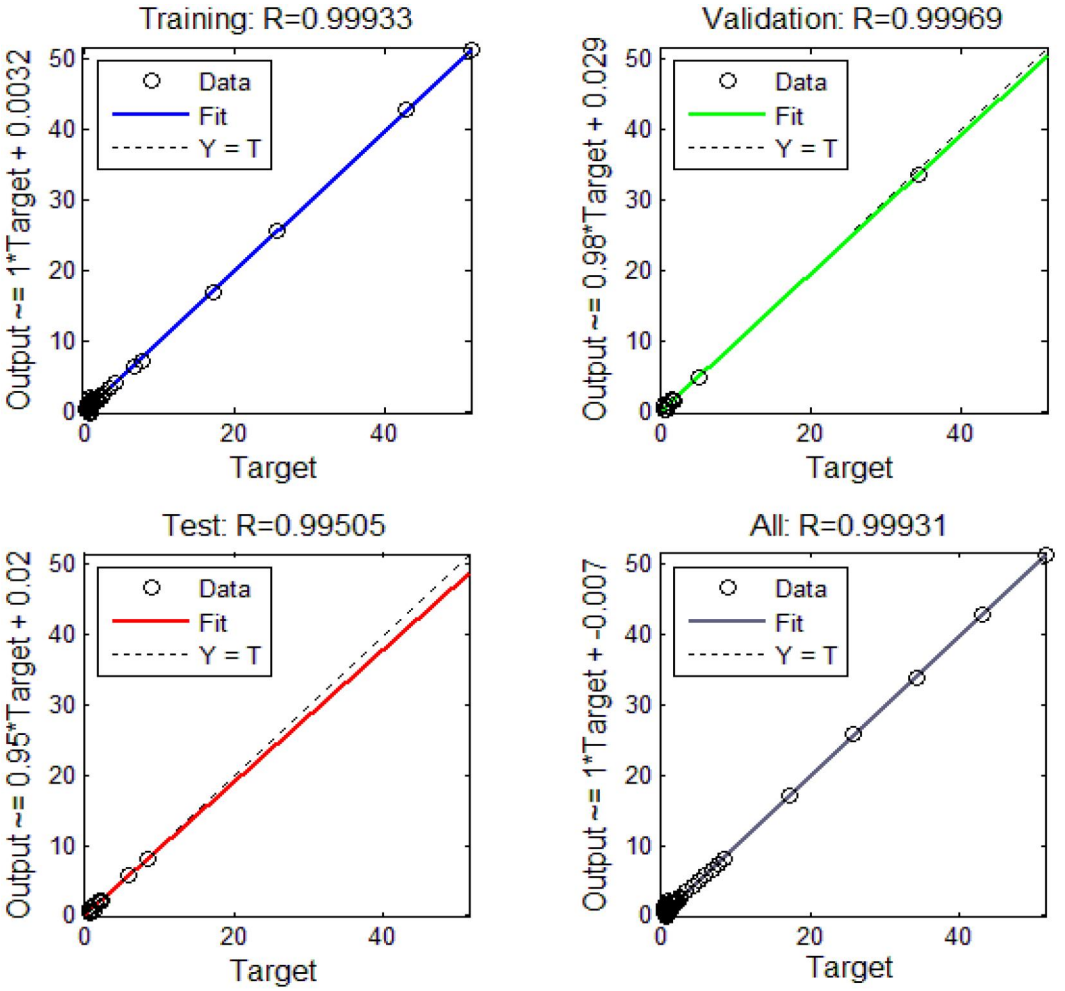

Figure 15. Regression values of neural network.

nanofluid temperature is higher when compared to nanofluid; this is due to the thermal conductivity of nanoparticles.

Variation of temperature profile for a hybrid, a nano- and a base fluid for various Eckert numbers in both channels is offered in Figure 5. An increase in Eckert number causes the transformation of kinetic energy into internal energy by work that is done against the viscous fluid stresses. Due to this, increasing Ec enhances the temperature of the fluid. The temperature of the hybrid nanofluid (MoS_2–MWCNTs/H_2O) is higher than that of the nanofluid (MoS_2/H_2O); this is because of the high thermal conductivity of nanoparticles.

Studying the influence of the thermal radiation parameter on temperature is the primary goal of the current investigation. The effect of thermal radiation on the temperature for both deviating and convergent canals is depicted in Figure 6. The radiation parameter rises as the temperature rises. This is because adding thermal radiation to the flow causes the fluid to warm up, raising the fluid's temperature. The heat of the hybrid nanofluid (MoS_2–MWCNTs/H_2O) is greater when compared to the nanofluid (MoS_2/H_2O).

From Figure 7*a*, the comparison between a hybrid, a nano- and a base fluid for temperature profile can be observed. The temperature of the base fluid is lower when compared to the nanofluid, this is due to the thermal conductivity of the nanoparticle. The temperature of the hybrid

Table 3. The water Prandtl number for atmospheric pressure at different temperatures.

State = fluid (water)		
Temperature		Prandtl number
(K)	(Celsius)	(–)
273	0	13.6
278	5	11.2
283	10	9.46
293	20	6.99
298	25	6.13
303	30	5.43
323	50	3.56
348	75	2.39
373	100	1.76

Table 4. Nu values toward Ec, Nr, and Pr.

Eckert number (Ec)	Nusselt number (Nu)	Radiation parameter (Nr)	Nusselt number (Nu)	Prandtl number (Pr)	Nusselt number (Nu)
0.01	0.8582	1	0.8995	7	0.8582
0.02	1.7163	2	0.8582	8	0.9807
0.03	2.5745	3	0.8204	9	1.1033
0.04	3.4326	4	0.7859	10	1.2259
0.05	4.2908	5	0.7541	11	1.3485
0.06	5.1489	6	0.7248	12	1.4711
0.07	6.0071	7	0.6977	13	1.5937
0.08	6.8652	8	0.6726	14	1.7163
0.09	7.7234	9	0.6492	15	1.8389
0.1	8.5815	10	0.6273	16	1.9615
0.2	17.1631	11	0.6069	17	2.0841
0.3	25.7446	12	0.5878	18	2.2067
0.4	34.3262	13	0.5698	19	2.3293
0.5	42.9077	14	0.5530	20	2.4519
0.6	51.4893	15	0.5370	21	2.5745

nanofluid is beyond that of the nanofluid, because of the thermal conductivity of the two nanoparticles. Figure 7*b* shows the comparison graph for the absence and presence of parameters and nanoparticles. In the occurrence of thermal radiation, it is noticed that 12% of the temperature of the nanofluid (MWCNTs/water) can be enhanced compared to that of base fluid; 14% of the temperature is enhanced in a hybrid nanofluid. This is due to the thermal conductivity of nanoparticles.

The Nusselt number graph for variation in Nr, Re, Ec, and α the divergent channel is shown in Figure 8. This graph is for hybrid nonfluid. By increasing Nr, Ec, and α, the heat transfer rate can be enhanced. The heat transfer rate decreases by increasing the Reynolds number.

A quadratic regression graph for magnetic and Reynolds numbers is depicted in Figures 9*a*, *b*. The regression line is closest to the data points as shown. Eq. (27) is fixed in this quadratic regression. By changing the values of M and Re in the regression equation, this statistical tool helps to study how skin friction behaves when the independent variables M and Re change. These figures show that skin friction is positively correlated with M and Re.

Figure 10 displays the graph of skin friction for M, Re, and α divergent channels. By increasing the Reynolds number, magnetic parameter, and angle of inclination, the skin friction coefficient also increases. This graph is plotted for a hybrid nanofluid.

Table 3 denotes the water Prandtl number for atmospheric pressure at different temperatures. By using this table, the quadratic regression chart is plotted for various values of Pr, which is observed in Figure 11*b*. For this quadratic regression, Eq. (30) is fixed. Figure 11*a* represents the quadratic regression graph for the Nusselt number with thermal radiation. From this graph, the

Table 5. Nu values toward Re and *M*.

Reynolds number (Re)	Nusselt number (Nu)	Magnetic parameter (*M*)	Nusselt number (Nu)
1	1.2116	1	0.4750
1.5	1.1838	2	0.8582
2	1.1518	3	1.1803
2.5	1.1154	4	1.3685
3	1.0742	5	1.5220
3.5	1.0281	6	1.6847
4	0.9768	7	1.8155
4.5	0.9202	8	1.8800
5	0.8582	9	1.8883
5.5	0.7907	10	1.8728
6	0.7177	11	1.8596
6.5	0.6394	12	1.8599
7	0.5558	13	1.8740
7.5	0.4673	14	1.8977
8	0.3740	15	1.9264

relation between the Nusselt number and thermal radiation can be observed. By changing the values of Nr and Pr in the regression equation, this statistical tool helps to study how the Nusselt number behaves when the independent variables Nr and Pr change. From these graphs, it is noticed that the Nusselt number is positively correlated with Nr and Pr.

4. ANN model

The Jeffrey Hamel flow [40, 41] is considered in the non-parallel plates. The heat transfer aspects are well-thought-out in the presence of thermal radiation and viscous dissipation effects. The Molybdenum disulfide nanoparticles are suspended in a flow regime. Various researchers [42–44] used ANN models to predict physical happenings. Due to this motivation, we evaluate the Nusselt number by using ANN on five various flow parameters. Figure 12 offers the architecture of the neural network.

The first layer owns the five inputs. The second layer is termed as the hidden layer and 15 neurons are considered in this layer. The last layer owns the Nusselt number (Nu) as an output value. The flow affecting parameters namely, the Eckert number, thermal radiation parameter, Prandtl number, Reynolds number, and magnetic field parameter being involved in flow narrating differential are selected as inputs. Turn wise, by varying one parameter and fixing the rest four, we collect complete set of data for Nusselt number. Further, by following the convergence factors, we restricted the outcomes to 75 as a sample data, see Tables 4 and 5. Such values are calculated by using DTM. The values that are less than unity correspond to higher conductive heat transfer while values that are greater than unity own higher convective heat transfer. The three different kinds of samples are considered, which include 53 (70%) values for training the neural network, 11 (15%) for testing and validation of the ANN model. The following are the transfer functions for hidden and output layers:

$$F_T(x) = \frac{1}{1 + e^{-x}} \tag{31}$$

$$\text{Pureline}(x) = x \tag{32}$$

Further, the training is done by using Levenberg–Marquardt backpropagation. The MSE and coefficient of determination (R), two performance indicators, are termed as follows:

$$\text{MSE} = \frac{1}{N}\sum_{i=1}^{N}\left(X_{\text{num}(i)} - X_{\text{ANN}(i)}\right)^2 \tag{33}$$

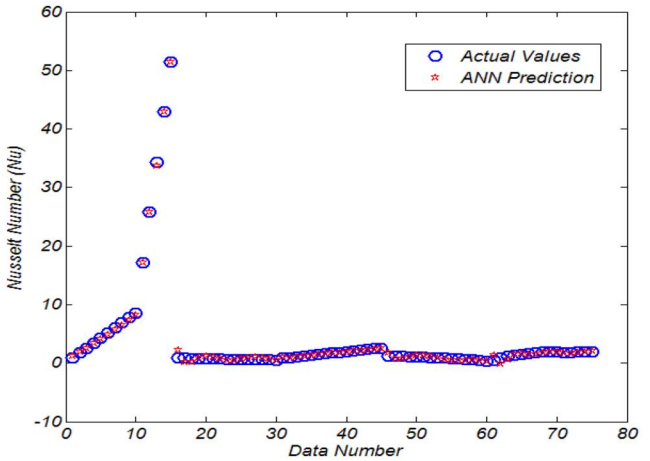

Figure 16. Comparison of ANN predicted and actual values.

Table 6. Performance indicators for ANN model.

Training	Validation	Test
MSE		
0.1210	0.0885	0.0780
R		
0.9993	0.9997	0.9951

$$R = \sqrt{1 - \frac{\sum_{i=1}^{N} \left(X_{\text{num}(i)} - X_{\text{ANN}(i)}\right)^2}{\sum_{i=1}^{N} \left(X_{\text{num}(i)}\right)^2}} \tag{34}$$

Figures 13–16 are the graphical outcomes by use of the ANN model. In detail, Figure 13 offers the performance of the neural network to predict the values of the Nusselt number. One can see the MSE values are high up to epoch 4, while for the upcoming epoch, the MSE reduces significantly. The best validation performance is obtained at 0.088537 at epoch 16. Figure 14 offers the error histogram with 20 bins. It can be seen that error values are very low, and hence the training of the neural networking model is completed with accuracy. Figure 15 offers the regression analysis with the help of graphs for all kinds of stages, namely testing, training, and validation. In detail, the regression value for the training is noted as $R = 0.99933$ which is close to $R = 1$. Hence the predicted values of the ANN model and actual values are strongly correlated.

The regression values for the validation are noted as $R = 0.99969$ and for testing, they are noted as $R = 0.99505$. Both are close to $R = 1$. Collectively, for all stages, we get $R = 0.99931$. Therefore, one can say that the actual Nusselt number and predicted values are correlated.

In Figure 16, predicted values for Nusselt numbers are compared to actual values using ANNs. One can see that the predicted values are in great agreement with the actual values of Nu. Therefore, the constructed neural networking model holds the capability to predict the Nusselt number values with accuracy. Table 6 gives the performance parameter for the ANN model. The MSE values for training, validation, and testing are low, which means we have negligible error while a strong correlation is directed by regression values.

5. Conclusion

In this study, the heat transfer aspects of Jeffery–Hamel hybrid nanofluid flow toward a convergent and divergent channel are inspected by using the differential transform approach. An ANN

model is used to predict the Nusselt number for five different flow parameters. The key outcomes are:

- The fluid flow for the hybrid nanofluid (MoS_2–MWCNTs/H_2O) and nanofluid (MoS_2/H_2O) is the same in both divergent ($\alpha > 0$) and convergent ($\alpha < 0$) channels.
- The velocity increases when the Reynolds number increases in the convergent channel ($\alpha < 0$), the reverse process is observed in the divergent channel ($\alpha > 0$).
- The temperature of MoS_2–MWCNTs/H_2O is higher when compared to MoS_2/H_2O.
- For training, testing, and validation, the regression value is noticed as $R = 0.99931$ and implies a strong correlation.
- MSE values are noticed significantly low, therefore the ANN predicted values are in great agreement with the actual values of Nu.
- Owning to a prediction by ANN, the Nusselt number is found to the increasing function of Ec, Pr, and M while the opposite is the case for Re and Nr.
- One can extend such idea to examine the non-Newtonian fluid flow fields (Carreau, Powell–Eyring, etc.) having engineering standpoints.

Acknowledgment

The authors would like to thank Prince Sultan University, Saudi Arabia, for the technical support through the TAS research lab.

Disclosure statement

No potential conflict of interest was reported by the author(s).

References

[1] G. B. Jeffery, "L. The two-dimensional steady motion of a viscous fluid," *Lond. Edinb. Dublin Philos. Mag. J. Sci.*, vol. 29, no. 172, pp. 455–465, Apr. 1915. DOI: 10.1080/14786440408635327.
[2] G. Hamel, "Spiral formige Bewegungen Zaher Flussigkeiten," *Math. Verein*, vol. 25, pp. 34–60, 1917.
[3] J. L. Fitzjohn and W. L. Holstein, "Divergent flow in chemical vapor deposition reactors," *J. Electrochem. Soc.*, vol. 137, no. 2, pp. 699–703, Feb. 1990. DOI: 10.1149/1.2086535.
[4] A. Vahabzadeh, D. D. Ganji, and M. Abbasi, "Analytical investigation of porous pin fins with variable section in fully-wet conditions," *Case Stud. Therm. Eng.*, vol. 5, pp. 1–12, Mar. 2015. DOI: 10.1016/j.csite.2014.11.002.
[5] M. Fakour, D. D. Ganji, and M. Abbasi, "Scrutiny of underdeveloped nanofluid MHD flow and heat conduction in a channel with porous walls," *Case Stud. Therm.Eng.*, vol. 4, pp. 202–214, Nov. 2014. DOI: 10.1016/j.csite.2014.10.003.
[6] J. Prins, "On the structure of compressor gas leakage flows," International Compressor Engineering Conference, Purdue University, Purdue e-Pubs, 2006.
[7] J. Peixinho, "Flow a slowly divergent pipe section," Seventh IUTAM Symposium on Laminar-Turbulent Transition, Springer, Dodrecht, 2010, pp. 307–312. DOI: 10.1007/978-90-481-3723-7_49.
[8] A. McAlpine and P. G. Drazin, "On the spatio-temporal development of small perturbations of Jeffery–Hamel flows," *Fluid Dyn. Res.*, vol. 22, no. 3, pp. 123–138, Mar. 1998. DOI: 10.1016/S0169-5983(97)00049-X.
[9] Z. Z. Ganji, D. D. Ganji, and M. Esmaeilpour, "Study on nonlinear Jeffery–Hamel flow by He's semi-analytical methods and comparison with numerical results," *Comput. Math. Appl.*, vol. 58, no. 11-12, pp. 2107–2116, Dec. 2009. DOI: 10.1016/j.camwa.2009.03.044.
[10] G. Domairry, A. Mohsenzadeh, and M. Famouri, "The application of homotopy analysis method to solve nonlinear differential equation governing Jeffery–Hamel flow," *Commun. Nonlinear Sci. Numer. Simul.*, vol. 14, no. 1, pp. 85–95, Jan. 2009. DOI: 10.1016/j.cnsns.2007.07.009.
[11] S. S. Motsa, P. Sibanda, F. G. Awad, and S. Shateyi, "A new spectral-homotopy analysis method for the MHD Jeffery–Hamel problem," *Comput. Fluids*, vol. 39, no. 7, pp. 1219–1225, Aug. 2010. DOI: 10.1016/j.compfluid.2010.03.004.

[12] O. D. Makinde and P. Y. Mhone, "Hermite–Padé approximation approach to MHD Jeffery–Hamel flows," *Appl. Math. Comput.*, vol. 181, no. 2, pp. 966–972, Oct. 2006. DOI: 10.1016/j.amc.2006.02.018.

[13] J. Prathap Kumar, J. C. Umavathi, and B. M. Biradar, "Mixed convection of magneto hydrodynamic and viscous fluid in a vertical channel," *Int. J. Non-Linear Mech.*, vol. 46, no. 1, pp. 278–285, Jan. 2011. DOI: 10.1016/j.ijnonlinmec.2010.09.008.

[14] A. Ishak, R. Nazar, and I. Pop, "MHD boundary-layer flow of a micropolar fluid past a wedge with constant wall heat flux," *Commun. Nonlinear Sci. Numer. Simul.*, vol. 14, no. 1, pp. 109–118, Jan. 2009. DOI: 10.1016/j.cnsns.2007.07.011.

[15] K. V. Prasad, D. Pal, and P. S. Datti, "MHD power-law fluid flow and heat transfer over a non-isothermal stretching sheet," *Commun. Nonlinear Sci. Numer. Simul.*, vol. 14, no. 5, pp. 2178–2189, May 2009. DOI: 10.1016/j.cnsns.2008.06.021.

[16] J. Umavathi and M. Shekar, "Effect of MHD on Jeffery–Hamel flow in nanofluids by differential transform method," *Int. J. Eng. Res. Appl.*, vol. 3, no. 5, pp. 953–962, 2013.

[17] M. Hatami, M. Sheikholeslami, M. Hosseini, and D. D. Ganji, "Analytical investigation of MHD nanofluid flow in non-parallel walls," *J. Mol. Liq.*, vol. 194, pp. 251–259, Jun. 2014. DOI: 10.1016/j.molliq.2014.03.002.

[18] F. O. Ochieng, M. N. Kinyanjui, and M. E. Kimathi, "Hydromagnetic Jeffery–Hamel unsteady flow of a dissipative non-Newtonian fluid with nonlinear viscosity and skin friction," *Glob. J. Pure Appl. Math.*, vol. 14, pp. 1101–1119, Nov. 2018.

[19] U. Rashid, A. Iqbal, H. Liang, W. Khan, and M. W. Ashraf, "Dynamics of water conveying zinc oxide through divergent-convergent channels with the effect of nanoparticles shape when Joule dissipation are significant," *PLoS One*, vol. 16, no. 1, p. e0245208, Jan. 2021. DOI: 10.1371/journal.pone.0245208.

[20] U. Khan *et al.*, "A novel hybrid model for Cu–Al_2O_3/H_2O nanofluid flow and heat transfer in convergent/divergent channels," *Energies*, vol. 13, no. 7, p. 1686, Apr. 2020. DOI: 10.3390/en13071686.

[21] R. Meher and N. D. Patel, "Analytical investigation of MHD Jeffery–Hamel flow problem with heat transfer by differential transform method," *SN Appl. Sci*, vol. 1, no. 7, p. 656, Jul. 2019. DOI: 10.1007/s42452-019-0632-z.

[22] R. Meher and N. D. Patel, "A study on magneto hydrodynamics Jeffery–Hamel flow with heat transfer problem in Eyring-Powell fluid using differential transform method," *J. Appl. Math. Comput. Mech.*, vol. 18, no. 3, pp. 57–68, Sep. 2019. DOI: 10.17512/jamcm.2019.3.05.

[23] H. Bilal *et al.*, "A Levenberg–Marquardt backpropagation method for unsteady squeezing flow of heat and mass transfer behaviour between parallel plates," *Adv. Mech. Eng.*, vol. 13, no. 10, p. 168781402110408, 2021. DOI: 10.1177/16878140211040897.

[24] I. Khan *et al.*, "Fractional analysis of MHD boundary layer flow over a stretching sheet in porous medium: a new stochastic method," *J. Funct. Spaces*, vol. 2021, pp. 1–19, 2021. DOI: 10.1155/2021/5844741.

[25] I. Khan *et al.*, "Falkner–Skan Equation with heat transfer: a new stochastic numerical approach," *Math. Probl. Eng*, vol. 2021, pp. 1–17, 2021. DOI: 10.1155/2021/3921481.

[26] M. Shoaib *et al.*, "Heat transfer impacts on maxwell nanofluid flow over a vertical moving surface with MHD using stochastic numerical technique via artificial neural networks," *Coatings*, vol. 11, no. 12, p. 1483, 2021. DOI: 10.3390/coatings11121483.

[27] H. Ullah *et al.*, "Modification of the optimal auxiliary function method for solving fractional order KdV equations," *Fractal Fract.*, vol. 6, no. 6, p. 288, 2022. DOI: 10.3390/fractalfract6060288.

[28] H. Ullah *et al.*, "Intelligent computing of Levenberg–Marquard technique backpropagation neural networks for numerical treatment of squeezing nanofluid flow between two circular plates," *Math. Probl. Eng.*, vol. 2022, pp. 1–11, 2022. DOI: 10.1155/2022/9451091.

[29] H. Ullah *et al.*, "Levenberg–Marquardt backpropagation for numerical treatment of micropolar flow in a porous channel with mass injection," *Complexity*, vol. 2021, pp. 1–12, 2021. DOI: 10.1155/2021/5337589.

[30] H. Ullah *et al.*, "MHD boundary layer flow over a stretching sheet: a new stochastic method," *Math. Probl. Eng.*, vol. 2021, pp. 1–26, 2021. DOI: 10.1155/2021/9924593.

[31] H. Ullah *et al.*, "Neuro-computing for hall current and MHD effects on the flow of micro-polar nano-fluid between two parallel rotating plates," *Arab. J. Sci. Eng.*, vol. 47, no. 12, pp. 16371–16391, 2022. DOI: 10.1007/s13369-022-06925-z.

[32] J. K. Zhou, *Differential Transformation and Its Applications for Electrical Circuits*. Wuhan: Huazhong University Press, 1986.

[33] A. S. V. Ravi Kanth and K. Aruna, "Two-dimensional differential transform method for solving linear and non-linear Schrödinger equations," *Chaos Solitons Fractals*, vol. 41, no. 5, pp. 2277–2281, Sep. 2009. DOI: 10.1016/j.chaos.2008.08.037.

[34] F. Ayaz, "Applications of differential transform method to differential-algebraic equations," *Appl. Math. Comput.*, vol. 152, no. 3, pp. 649–657, May 2004. DOI: 10.1016/S0096-3003(03)00581-2.

[35] H. Berrehal and G. Sowmya, "Heat transfer analysis of nanofluid flow in a channel with non-parallel walls," *J. Mech. Sci. Technol.*, vol. 35, no. 1, pp. 171–177, Jan. 2021. DOI: 10.1007/s12206-020-1216-y.

[36] E. Abu-Nada, "Application of nanofluids for heat transfer enhancement of separated flows encountered in a backward facing step," *Int. J. Heat Fluid Flow*, vol. 29, no. 1, pp. 242–249, Feb. 2008. DOI: 10.1016/j.ijheatfluidflow.2007.07.001.

[37] H. Sadaf, Z. Asghar, and N. Iftikhar, "Cilia-driven flow analysis of cross fluid model in a horizontal channel," *Comput. Part. Mech.*, vol. 10, no. 4, pp. 943–950, 2023. DOI: 10.1007/s40571-022-00539-w.

[38] Y. Nawaz, M. S. Arif, and K. Abodayeh, "Predictor–corrector scheme for electrical magnetohydrodynamic (MHD) Casson nanofluid flow: a computational study," *App. Sci.*, vol. 13, no. 2, pp. 1209, 2023. DOI: 10.3390/app13021209.

[39] Y. Nawaz, M. S. Arif, K. Abodayeh, and M. Mansoor, "Finite difference schemes for MHD mixed convective Darcy–Forchheimer flow of non-Newtonian fluid over oscillatory sheet: A computational study," *Front. Phys.*, vol. 11, 2023. DOI: 10.3389/fphy.2023.1072296.

[40] S. Rehman *et al.*, "A generalization of Jeffrey-Hamel problem to Reiner-Rivlin model for energy and thermodynamic analysis using Keller-Box computational framework," *Case Stud. Therm. Eng.*, vol. 50, p. 103462, 2023). DOI: 10.1016/j.csite.2023.103462.

[41] P. Chandra and R. Das, "A hybrid RSA-IPA optimizer for designing an artificial neural network to study the Jeffery–Hamel blood flow with copper nanoparticles: application to stenotic tapering artery," *Results Eng.*, vol. 20, p. 101542, 2023. DOI: 10.1016/j.rineng.2023.101542.

[42] S. A. Kalogirou, "Applications of artificial neural-networks for energy systems," *Appl. Energy*, vol. 67, no. 1–2, pp. 17–35, 2000. DOI: 10.1016/S0306-2619(00)00005-2.

[43] K. U. Rehman, W. Shatanawi, and A. B. Çolak, "Computational analysis on magnetized and non-magnetized boundary layer flow of Casson fluid past a cylindrical surface by using artificial neural networking," *Math*, vol. 11, no. 2, p. 326, 2023. DOI: 10.3390/math11020326.

[44] S. Wen, M. W. Lee, K. M. K. Bastos, I. K. Eldridge-Allegra, and E. H. Dowell, "Feature identification in complex fluid flows by convolutional neural networks," *Theor. Appl. Mech. Lett.*, vol. 13, no. 6, p. 100482, 2023. DOI: 10.1016/j.taml.2023.100482.